Urban Black-Odor Water Remote Sensing Mapping Based on Shadow Removal: A Case Study in Nanjing

Taixia Wu, Mengyao Li, Shudong Wang, Yingying Yang, Shan Sang, and Dongzhen Jia

***Abstract*—Urban black-odor water is a serious water environmental problem worldwide that seriously affects the living environment and the health of residents. The detection of black-odor water is a primary problem of centralized governance. Remote sensing is an effective means for water-quality monitoring. However, in most urban areas, with their complex underlying conditions, black-odor water always shows an uncertain distribution and small area. Furthermore, because of similar spectral characteristics, it is easily confused with dark objects such as asphalt roads, dark roofs, bridges, river levees, and building shadows. In this article, we propose a new black-odor water detection method, without shadow misjudgment, for complex urban conditions. A remote sensing image from the Chinese high-resolution satellite Gaofen-2 (GF-2) was used for detection. Using *in situ* water-quality measurement data for verification, the results showed that the proposed method achieved an accuracy of 85.7% while reducing the false alarm rate to 3.5%. Compared to four other existing methods, the proposed method proved to be more practical because it can reduce the false extraction of nonblack-odor water to the greatest extent possible while ensuring accuracy The method proposed in this article has a good effect on the extraction of black-odor water in Nanjing City. Therefore, our method can be applied widely to screening and management of large-scale urban black-odor water and can provide reliable data for centralized treatment.**

***Index Terms*—Complex underlay, GF-2, remote sensing, shadow, urban black-odor water.**

I. Introduction

BLACK-ODOR water (BOW) refers to water with an unpleasant color and/or odor [1]. Urban BOW is a product of the process of industrialization and is caused mainly by the discharge of pollutants [2] and noncirculation of the water itself. In recent years, BOW has severely affected the living environment of urban residents and presented great challenges to the urban water ecosystem. BOW not only affects the beauty of cities but also may pollute soil, groundwater resources, and even sources of domestic and drinking water, which seriously threatens human health. Therefore, centralized control of BOW is vitally important, and the discovery of these waters is the first step. According to the 2015 *China Environmental Bulletin*, BOW accounts for 8.8% of the more than 900 sections under state control and monitoring in key waters across the country. The Chinese government has issued a series of policies and documents pertaining to the investigation of BOW since 2015 [3]. Among these, the "Action Plan for Water Pollution Prevention and Control" issued by the State Council in 2015 required urban built-up areas to complete water quality screening by the end of 2015, begin eliminating BOW by the end of 2017, and generally eliminate BOW by the end of 2030. Therefore, the detection of urban BOW is extremely urgent. However, there are still many technical difficulties in the detection of BOW. Most urban BOWs are elongated rivers and round ponds with a dark color and small area. Some of them are temporary but others are perennial. These features make it difficult to achieve accurate and large-scale detection in a short time. The traditional detection method requires measurement of water quality, which not only must overcome the difficulties of field measurement but requires a lot of money, labor, and time. Therefore, a more accurate and practical way to monitor the distribution of BOW needs to be identified.

Remote sensing technology can be used to identify a wide range of objects quickly [4]–[6]; thus, it is advantageous to use it for detection of BOW. However, research in this area is still in its infancy. Although many studies have used remote sensing technology to analyze water quality [7]–[9] and water quality parameters [10]–[12], few have focused on BOW. Most of the existing studies on BOW are about the characteristics [13], [14], causes [15], [16], biochemical mechanism [17]–[19], and treatment of BOW [20], [21]. Only a few studies have considered the detection and identification of BOW by remote sensing technology. Shen *et al*. [22] summarized the difficult problems and key technologies of remote sensing monitoring of BOW. The key technologies are image pretreatment technology, water extraction technology, BOW classification technology, and the identification model of BOW based on a remote sensing platform. Their work provides general direction for remote sensing monitoring of BOW. Jin and Pan [23] used remote sensing to assess BOW in the nine rivers in Beijing by extracting the river water boundary and retrieving water-quality parameters from Gaofen-2 (GF-2) fusion imagery. The results were almost consistent with the official results. Wen *et al*. [24] constructed four remote sensing recognition algorithms for BOW based on analyses of measured water surface spectral data by the single-band

Manuscript received May 15, 2021; revised August 18, 2021; accepted September 14, 2021. Date of publication September 21, 2021; date of current version October 6, 2021. This work was supported in part by the Specially Appointed Professor Program of Jiangsu Province under Grant 41671362 and in part by the National Natural Science Foundation of China under Grant 41371359. *(Taixia Wu and Mengyao Li are co-first authors.) (Corresponding author: Shudong Wang.)*

Taixia Wu, Mengyao Li, Yingying Yang, Shan Sang, and Dongzhen Jia are with the School of Earth Sciences and Engineering, Hohai University, Nanjing 210098, China (e-mail: wutx@hhu.edu.cn; limy@hhu.edu.cn; yyy@hhu.edu.cn; sangshan@hhu.edu.cn; jdz@hhu.edu.cn).

Shudong Wang is with the Aerospace Information Research Institute, Chinese Academy of Sciences, Beijing 100101, China (e-mail: wangsd@radi.ac.cn).

Digital Object Identifier 10.1109/JSTARS.2021.3114355

threshold method, band difference method, band ratio method, and chromaticity method. The band ratio method had the highest accuracy. Yao *et al*. [25] proposed the black and odorous water index (BOI) to detect BOW based on the band ratio method. Li *et al*. [26] proposed a water cleanliness index (WCI) to reflect the degree of cleanliness from spectral characteristics and constructed interpretation marks from image features, such as water color, secondary environment, river channel siltation, and littoral garbage stacking. They used the above two methods to identify BOW. Shen *et al*. [2] divided BOW into two types, one with high concentrations of iron sulfide and another with high concentrations of total suspended matter, and then proposed a Commission Internationale de L 'Eclairage (CIE) color purity algorithm to distinguish these from ordinary water. They achieved good results. These studies proposed various methods for distinguishing BOW from ordinary water and made great progress. However, there are still many problems associated with detecting BOW. As most large areas of open water are active water bodies that generally self-purify, these areas do not become BOWs. BOWs are often narrow rivers and small ponds, and detection of these waters is limited by satellite resolution (including spatial, temporal, and spectral resolutions), the accuracy of algorithms, the complexity of the underlying conditions, and the characteristics of the BOW [2]. However, the identification methods of BOW proposed in the aforementioned studies have two main problems. First, due to the differences in the formation mechanisms of BOW, the spectral information of BOW in different regions and seasons also differs. The identification method of BOW in the above study is difficult to apply to all types of BOW. Therefore, it is necessary to propose a more general identification index for BOW. Second, it is more difficult to detect urban BOW because the urban underlying condition is very complex. For example, asphalt roads, roofs, dams, bridges, and particularly shadows are easily confused with BOWs in remote sensing images. However, the aforementioned studies did not solve the problem of confusing BOW with other background features. They only distinguished ordinary water from BOW. In practical applications, it is necessary to obtain accurate water boundaries to accurately extract BOW. Due to the low reflectance and narrow shape and area of BOW, the existing water extraction methods cannot fully meet the accuracy requirements needed to detect BOW. Therefore, most of the above studies also needed to manually digitize the water boundary. To solve these problems, it is necessary to propose a BOW mapping method that can effectively suppress background elements in the high-resolution image and is suitable for the complex underlying areas of urban regions.

To map BOW under the condition of a complex underlying surface, in addition to the problem of distinguishing BOW from ordinary water, there is the more difficult problem of the influence of complex background factors on the extraction of BOW during the extraction of the water boundary. Of all the complex background elements, shadows are most difficult to distinguish from BOW. Due to their low reflectance, water, and especially BOW are easily confused with shadows in remote sensing images, which is a key problem for detecting BOWs. The brightness values of shadow and BOW are very similar in all bands of remote sensing images, and misjudgment of shadow has the greatest influence on the recognition of BOW. Many studies have examined shadow removal. Shadows can be detected using many different methods, including color space transformation [27]–[29], the construction of a shadow index via band calculation [30]–[34], machine learning [35]–[37], and the illumination model [38]–[40]. However, these shadow-removal strategies have some disadvantages in practical applications. For example, color space transformation and the shadow index can usually remove most shadows, but many finely broken shadow spots remain, and those remaining spots still have a great impact on ground object recognition. Machine learning often requires the collection of a large number of samples and the manual setting of various complex parameters, so this method cannot be applied in practical applications. The illumination model requires complex solar and sensor parameters, so it too is not easy to apply. Therefore, to carry out remote sensing mapping of BOW more accurately, it is necessary to find a more convenient and practical method to remove the influence of shadows on the recognition results.

In this study, we used GF-2 high-resolution satellite imagery to detect BOW under complex conditions. We had two major objectives. The first was to propose a new and more general identification index of BOW. The second was to solve the problem of misjudgment caused by low-reflectance objects such as shadows in remote sensing detection of BOW and realize high-precision remote sensing detection of BOW in large areas with complex underlying conditions.

II. Study Area and Data

A. Study Area and Distribution of in Situ Samples

This study selected Nanjing, a representative Chinese city, as the study area. Nanjing, within Jiangsu Province, is located in the densely populated eastern part of China. With the rapid development of industry, the city's environmental problems are becoming progressively more acute. The climate in Nanjing is a typical north subtropical humid climate with four distinct seasons. The city has abundant water resources, including 821 river channels, 251 reservoirs, and 10 lakes. The water area accounts for 11.4% of the total area. The abundant rivers and lakes should provide a high-quality living environment to urban residents; however, with the increase in urbanization, water pollution has become a serious concern for the government, which has issued corresponding policies to improve the water environment. We selected a location in the central part of the city of Nanjing, where BOWs, mostly small ponds and narrow rivers, are concentrated. Due to the poor infrastructure, there is no unified drainage pipe, and the sewage from surrounding residents is emptied into the water. Over time, the water here became black and odorous. The water quality is cloudy, the smell is bad, and some of the water supports floating algae, seriously affecting the lives of surrounding residents (Fig. 1). The study area contains common scenes in Chinese cities, including natural features such as water, woodland, farmland, and grassland, and artificial features such as buildings, roads, and bridges. Because the study area covers a variety of complex feature types and is a typical microcosm of urban China, with strong representativeness, it is suitable for

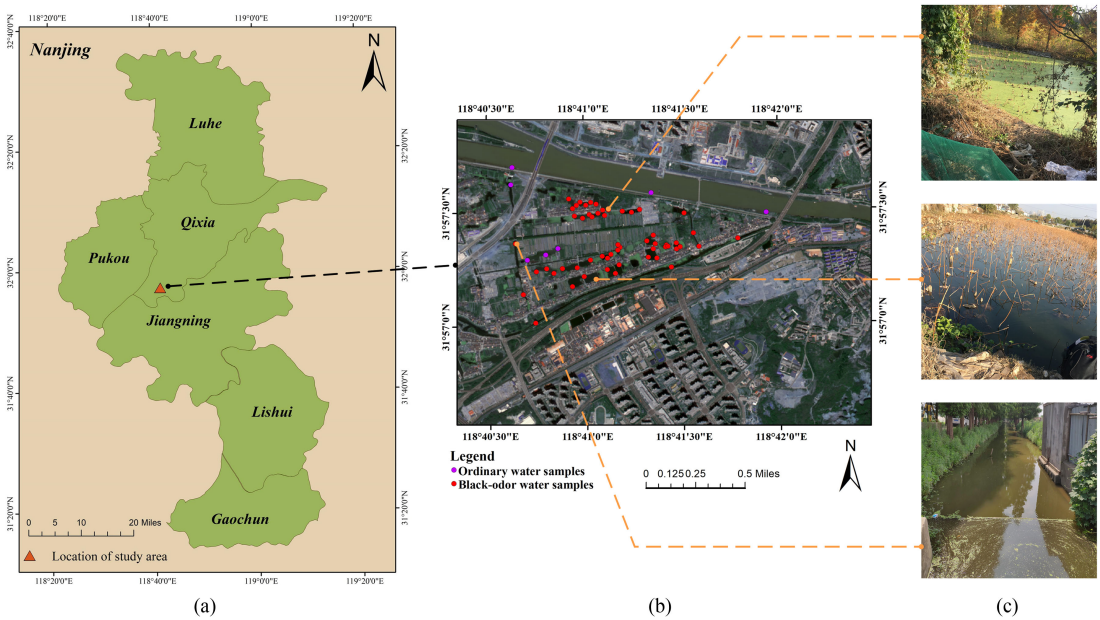

Fig. 1. (a) Location of the study area. (b) Distribution of field validation sampling points. To test the accuracy of the BOW detection model, 63 water samples were selected. The purple points are the ordinary water samples; the red points are the BOW samples. (c) The field conditions of three typical BOWs in the study area. The colors of the three typical BOWs are black, green, and brown, respectively.

TABLE I
CRITERIA AND METHODS FOR FIELD VALIDATION OF BOW

Characteristic index (units)	Moderate BOW	Severe BOW	Assay method	Notes
Transparency (cm)	25–10	<10	Secchi disk	In situ determination
Dissolved oxygen (mg/L)	0.2–2.0	<0.2	Electrochemical means	In situ determination
Redox potential (mV)	–200 to 50	< –200	Electrode method	In situ determination
Ammonia nitrogen (mg/L)	8.0-15	>15	Nessler's reagent photometric method/ Salicylic acid-hypochlorite photometric method	The water sample should be filtered through a 0.45μm membrane

the detection experiment of BOW under complex underlying surface.

We traveled to the study area to acquire the synchronous validation data on April 9, 2018. We measured a total of 63 sample points, as shown in Fig. 1(b), among which 56 points were BOW and 7 points were clear water. According to the grading standard of BOW and the determination methods of water-quality indicators provided by the Ministry of Housing and Urban–Rural Development of China [3], we selected three indicators for verification of BOW, as shown in Table I.

We measured the transparency of the water using a Secchi disk with a diameter of 20 cm. The dissolved oxygen (DO) content was measured using a JPB-607A portable DO meter, the redox potential was measured using a CT-8022 portable oxidation reduction potential (ORP) meter, and the water hyperspectral data were measured using an ASD FieldSpec3 spectrometer (Analytical Spectral Devices, USA). In addition, water samples collected at the site were kept in cold storage and taken to the laboratory to measure ammonia nitrogen.

B. Satellite Data and Processing

We selected a GF-2 image acquired on a sunny day at the study site on April 9, 2018. The GF-2 satellite is the first civil optical satellite developed by China with a spatial resolution better than 1 m. It is equipped with two high-resolution 1-m panchromatic cameras and one 4-m multispectral camera. The multispectral image provided by GF-2 includes four bands, namely, the blue, green, red, and near-infrared bands. The other parameters of GF-2 are shown in Table II.

The multispectral image from GF-2 was used in our BOW extraction experiment. We used the Environment for Visualizing Images (ENVI) software for image preprocessing, including orthorectification, followed by radiometric calibration, and, finally, fast line-of-sight atmospheric analysis of spectral hypercubes atmospheric correction to obtain the reflectance image of our study area. The ground-measured reflectance values synchronized with the satellite data were fitted to four bands of the GF-2 sensor by spectral response function, and compared with the GF-2 image after atmospheric correction. The fitting R^2 of atmospheric correction values and measured values in each band are all above 0.9.

III. METHODOLOGY

A flowchart of our research method is provided in Fig. 2. We first used the single-band threshold method to detect water from preprocessed images. On the basis of the water extraction, the

TABLE II
GF-2 SATELLITE PARAMETERS

Load	Band	Wavelength range (μm)	Spatial resolution (m)	Revisit time (days)
Panchromatic	PAN	0.45–0.90	1	5
Multispectral camera	Blue	0.45–0.52	4	
	Green	0.52–0.59		
	Red	0.63–0.69		
	Near infrared	0.77–0.89		

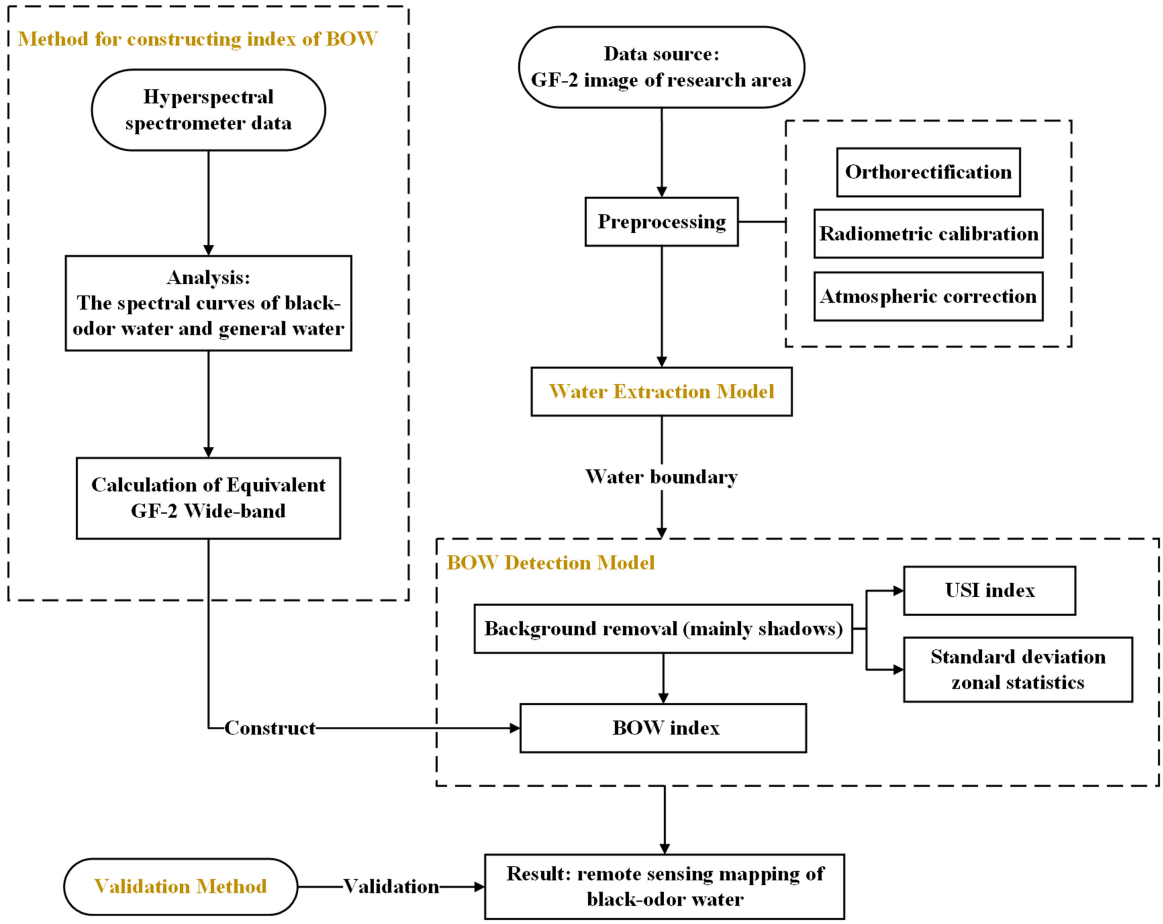

Fig. 2. Flowchart of BOW detection and evaluation of precision.

model constructed in this article was used to detect BOW. This method consists of two parts: distinguishing BOW from ordinary water and eliminating shadow effects. Finally, field validation data was used to verify the accuracy of the results.

A. Water Extraction Model

The single-band threshold method [41] is a simple and convenient method for extracting water. It uses the principle that the reflectance of water is lower than those of other ground objects in the near-infrared band to extract water. This method effectively removes land and water boundaries, but it retains many shadows. The specific parameters of the single-band threshold model are described as follows:

$$b_4 < t \tag{1}$$

where b_4 is the reflectance data of the GF-2 image in the near-infrared band expanded by 10000 times and t is the set threshold for extracting water. In this study, $t = 1160$ was selected as the threshold value for water extraction.

B. Method for Constructing the BOW Index

To distinguish ordinary water from BOW well, we must construct an index to detect BOW. We collated and analyzed *in situ* hyperspectral resolution reflectance data of BOW and ordinary water collected by the ASD spectrometer and then calculated their equivalent GF-2 wide-band values. According to the spectral response function of the GF-2 satellite, the remote sensing reflectance R_{rs} measured in the field with a spectral resolution of 1 m was converted into the wide band of the GF-2

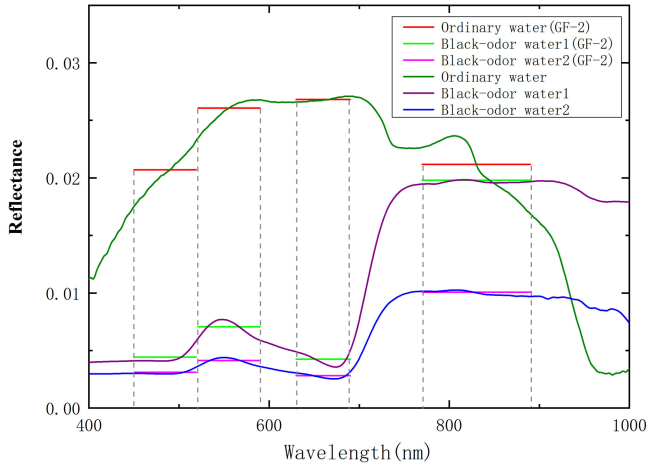

Fig. 3. Spectrum curves of the typical underlying surfaces in the study area overlapped with GF-2 bands. The continuous spectrum curves were measured using a spectrometer, and the short horizontal lines are the first four GF-2 equivalent wide bands of the corresponding underlying surfaces. The continuous curve above represents the spectral curve of ordinary water, which was calculated from the average spectral curve of several ordinary water samples. The two continuous curves below represent the spectral curves of two types of BOW, which were calculated by averaging the spectral curves of two different types of BOW samples.

image. The conversion formula is as follows [42]:

$$R_{\mathrm{eq}}(\lambda_i) = \frac{\int R_{\mathrm{rs}}(\lambda) f_i(\lambda) F_0(\lambda) d(\lambda)}{\int f_i(\lambda) F_0(\lambda) d(\lambda)} \tag{2}$$

where $R_{\mathrm{eq}}(\lambda_i)$ is the simulated equivalent reflectance of the ith GF-2 band, $R_{\mathrm{rs}}(\lambda)$ is the measured remote sensing spectral data, $f_i(\lambda)$ represents the spectral response function of each GF-2 band, and $F_0(\lambda)$ is the solar spectral irradiance beyond the atmosphere.

We calculated the average values of the collected spectra of different types of water. The spectral curves are shown in Fig. 3. Then, we used the spectral response function of the GF-2 satellite to simulate these as GF-2 wide-band equivalent reflectance, as shown by the short horizontal lines in Fig. 3. Spectral curves differed between ordinary water and BOW. As a whole, the reflectance of ordinary water was higher than that of BOW in the range of 400–700 nm, whereas that of BOW was relatively higher in the range of 700–1000 nm. More specifically, the BOW reflectance spectrum had a small reflection peak near the green band and increased obviously in the near-infrared band, while the variation in the spectrum of ordinary water reached its highest value near the green and red bands and decreased slowly in the near-infrared band. Therefore, these two types of water could clearly be distinguished. The BOW detection index was constructed as follows:

$$(B_G - B_B) \cdot (B_G - B_{NIR}) < h \tag{3}$$

where B_B, B_G, and B_{NIR} are the blue, green, and near-infrared bands of GF-2 data, respectively, and h is the threshold value of the artificially determined band calculation result. According to the spectral characteristics of the modeling sample points, $h = 10000$ was selected as the threshold to distinguish BOW from ordinary water. The threshold can also be adjusted around 10000 depending on the actual situation. The term $(B_G - B_{NIR})$ is the difference between the green and near-infrared bands in the spectral curves of the two kinds of water. As the BOW spectral curves are obviously elevated in the near-infrared band, values for BOW should be negative and those for ordinary water should be positive. However, in the GF-2 image, we observed that this value of some BOWs was positive and that the value of the near-infrared band was slightly lower than the value of the green band. In this case, the term $(B_G - B_B)$, which is the difference between the blue and green bands in the spectral curves of BOW and ordinary water, plays a greater role. Most of the BOW values were lower than those of ordinary water. When the two terms above were multiplied, the value of BOW was usually less than that of ordinary water.

C. BOW Detection Model

The water extracted by the single-band threshold method usually includes three types of ground objects, specifically, shadow, ordinary water, and BOW. The BOW detection model first removes the shadow and then separates the BOW from the ordinary water. The model is constructed as follows:

$$BOW = SDorWT \cap OW \quad \text{or} \quad BOW \tag{4}$$

where *BOW*, *SDorWT*, and *OWorBOW* are the values of pixels on a binary image. The *BOW* value is 1 when a pixel belongs to BOW, and it is 0 otherwise. The variable *SDorWT* indicates whether a pixel belongs to background or water. The *SDorWT* value is 1 if the pixel belongs to water, otherwise it is 0. The variable *OWorBOW* indicates whether a pixel belongs to ordinary water or BOW. The *OWorBOW* value is 1 if the pixel belongs to BOW, otherwise it is 0.

Therefore, the most important aspect of this BOW detection model is to determine the pixel values of *SDorWT* and *OWorBOW* binary images. The binary image *SDorWT* is obtained by removing shadow, and the binary image *OWorBOW* is obtained by removing the ordinary water through the BOW index.

1) Shadow Removal (SDorWT): **Step 1**: Using the urban shadow index (USI) to identify and remove shadow.

To separate water from shadow effectively, the USI [34] for high-resolution remote sensing images was used to remove shadow on a large scale. However, if the shadow is removed directly by calculating the USI pixel by pixel and setting the threshold, the final extraction result of BOW will be affected. Due to the common existence of different objects with the same spectral characteristics and the same object with different spectral characteristics, even after strict radiometric correction, there were still some abnormal pixel values. When the USI is directly used for shadow extraction, it is inevitable that individual pixels will be misclassified, which causes many problems. For example, the extracted shadow boundary is not complete enough, resulting in the remaining portion being mistakenly divided into BOW, which increases the false alarm rate. Some pixels in the BOW were misclassified as shadows, resulting in the hollow phenomenon of BOW in the mapping results, and the complete boundary could not be obtained. Therefore, we used

the water boundary extracted by the water extraction model as the constraint, calculated the average value of the USI inside each water boundary, and then set the threshold to remove most of the shadows. The method of shadow removal using the USI is as follows:

$$USI = 0.25 \cdot \frac{Pixel_{Bg}}{Pixel_{Br}} - 0.57 \cdot \frac{Pixel_{Bnir}}{Pixel_{Bg}} - 0.83 \cdot \frac{Pixel_{Bb}}{Pixel_{Bg}} + 1.0 \quad (5)$$

where $Pixel_{Bb}$, $Pixel_{Bg}$, $Pixel_{Br}$, and $Pixel_{Bnir}$ are the values of the same pixel in the images of the blue, green, red, and near-infrared bands of the GF-2 image, respectively.

Step 2: Calculating the variance within the constraint boundary to remove shadow.

For shadows that cannot be eliminated by the USI, Fang *et al*. [30] proposed that dark water and shadows can be distinguished by variance. This is based on the shadow projection on different underlying surfaces of higher complexity than the water surface. First, the red, green, and blue bands of the GF-2 image are preprocessed by low-pass filtering and normalization. The normalization method is shown in (6). The purpose of low-pass filtering is to smooth the image and reduce abnormal pixel values in water and shadow areas, and the purpose of normalization is to provide standard images for the calculation of standard deviation.

$$b_i = \frac{band_i - \min(band_i)}{\max(band_i) - \min(band_i)} \quad (6)$$

In the above, b_i ($i = 3$) is the standard value, $band_i$ is the filtered value, and $\max(band_i)$ and $\max(band_i)$ are the minimum and maximum values of $band_i$, respectively.

In the preprocessed single-band red, green, and blue images, the water boundary extracted by the water extraction model was used as the boundary to calculate the standard deviation of the pixels within each boundary. As the texture of the underlying surface projected by the shadow is relatively complex, whereas the texture of the water surface is relatively smooth, the standard deviation of the shadow is large and the standard deviation of the water is small. The reason the boundary is used as the constraint in calculation is that the standard deviation calculated within each water boundary will be the same value, the shadow will be completely removed, and there will be no broken polygons that cannot be removed. The standard deviation zonal statistical images of the three bands are added together as follows:

$$sd = Pixel_{B1} + Pixel_{B2} + Pixel_{B3} \quad (7)$$

where $Pixel_{B1}$, $Pixel_{B2}$, and $Pixel_{B3}$ are the results of standard deviation partition statistics of GF-2 images in blue, green, and red bands within the boundary of water.

The USI image calculated by step 1 and the *sd* image calculated by step 2 are used to construct the following methods to determine the value of *SDorWT*:

$$SDorWT = \begin{cases} 1, & (USI > w_1) \wedge (st < w_2) \\ 0, & \text{others} \end{cases} \quad (8)$$

where w_1 and w_2 are the thresholds used to distinguish the water from the shadow on the image of the calculated result of the band. Based on the brightness of the current image, the empirical thresholds were modified slightly. Hence, $w_1 = 0$ and $w_2 = 0.04$ were selected as the threshold values to distinguish water from background.

2) BOW Index (OWorBOW): By analyzing the wave reflection curves of general water and BOW, a new BOW index was constructed in Section III-B. The method, shown in (9) and (10), was constructed to determine the value of *OWorBOW*

$$p = (Pixel_{Rg} - Pixel_{Rnir}) \cdot (Pixel_{Rg} - Pixel_{Rb}) \quad (9)$$

$$OW\text{or}BOW = \begin{cases} 1, & p < h \\ 0, & p \geq h \end{cases} \quad (10)$$

where $Pixel_{Rg}$, $Pixel_{Rnir}$, and $Pixel_{Rb}$ are the values of a pixel in the green, near-infrared, and blue bands of the preprocessed GF-2 image, respectively, and *h* is the threshold value of the artificially determined band calculation result.

D. Validation Method

To verify the results of the proposed method, the following target detection method was adopted:

$$\text{AR} = \frac{(TT + FF)}{T + F} \times 100\% \quad (11)$$

$$\text{FAR} = \frac{TF}{(T + F)} \times 100\% \quad (12)$$

where AR and FAR represent the accuracy and false alarm rate, respectively. *T* is the number of samples for the actual target, and *F* is the number of samples for the actual nontarget. *TT* is the number of samples for targets detected correctly by the model, and *FF* is the number of targets that are actually nontargets and are not detected as targets. *TF* is the number of targets that are actually not targets but are detected as targets.

IV. Results

A. Threshold Selection for GF-2 Image

The method proposed in this article involves the selection of multiple thresholds. First, to determine the threshold *t* in the water extraction model accurately, a large number of sample points of water and nonwater on the GF-2 image covering the study area are randomly selected and their pixel values in the near-infrared band are counted. Considering that the integrity of the water boundary affects the subsequent calculation, we require a threshold that is as large as possible while still ensuring accuracy. Therefore, $t = 1160$ is the best threshold for water extraction from GF-2 images. However, due to the differences in brightness, region, and season of different images, this threshold can be adjusted slightly according to specific conditions.

Second, three thresholds need to be determined in the BOW detection model, namely, the threshold of the USI w_1, the threshold of the standard deviation calculation result w_2, and the threshold of the BOW index *h*. The thresholds w_1 and w_2 are selected according to the empirical threshold based on the brightness of the current image. Finally, $w_1 = 0$ and $w_2 = 0.04$ are the recommended values. To select a more accurate threshold *h*, high spectral resolution reflectance data of a large

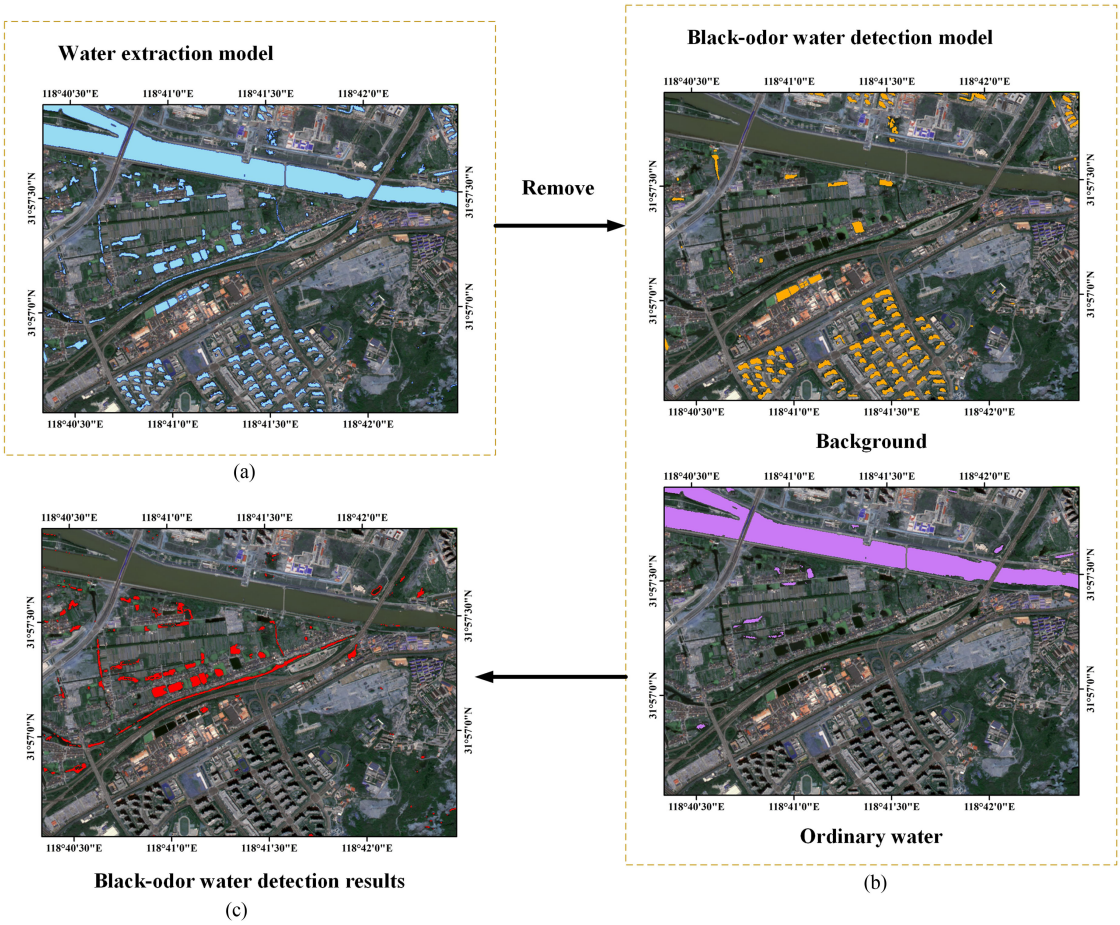

Fig. 4. Results of each stage of the experiment. First, the water (a) is extracted by the water extraction model. Second, the BOW (b) is extracted by the BOW extraction model, including the background removal and the distinction between BOW and ordinary water. Finally, the extraction result of the BOW (c) is obtained.

number of BOW and ordinary water samples are analyzed. Then, the GF-2 equivalent wide band of these sample points is calculated. As a result, $h = 10000$ is the best threshold after statistics. The sample points used to determine the threshold were collected from the study area. To further validate the suitability of the threshold, we carried out a large-scale experiment in Section IV-D for Nanjing, Qiqihaer, and Shenyang, three cities in different provinces with a large difference in latitude, and the results show that the selection of the threshold is universal.

B. Detection Results of BOW and Field Validation

Fig. 4 shows our detection result. For the water extraction result, the BOW detection model was used to remove the background and ordinary water. Then, a warning map of the distribution of BOW was obtained. To verify the BOW detection results, 63 water sampling points were selected after considering scientific aspects, accessibility, and safety. We detected BOW based on water extraction results, which contained three kinds of ground objects: ordinary water, BOW, and background (mostly shadows). Through visual interpretation, it could be determined that the real water in the polygon of the extracted water result was about three times that of the background polygon. Therefore, we randomly set 21 background sampling points to verify BOW detection accuracy. The setting and distribution of sampling points are shown in Table III and Fig. 5(a), respectively. According to formulas (6) and (7), the accuracy of the proposed detection model was 85.7% and the error rate was 3.5%.

TABLE III
SETTING OF THE GROUND SAMPLING POINTS

Type	Count
BOW samples	56
Ordinary water samples	7
Shadow samples	21

C. Comparison With Existing Models

We compared our model with the existing authoritative BOW model. The detection ability of each model is shown in Fig. 5, and the accuracies are shown in Table IV. By using the model proposed in this article, a detection accuracy of BOW of 85.7% can be attained, whereas other methods can reach only 50–60%. At the same time, we tried to reduce the false alarm rate as much as possible. Our false alarm rate was only 3.5%, while the false alarm rate of other methods was as high as 20–30%. A high false

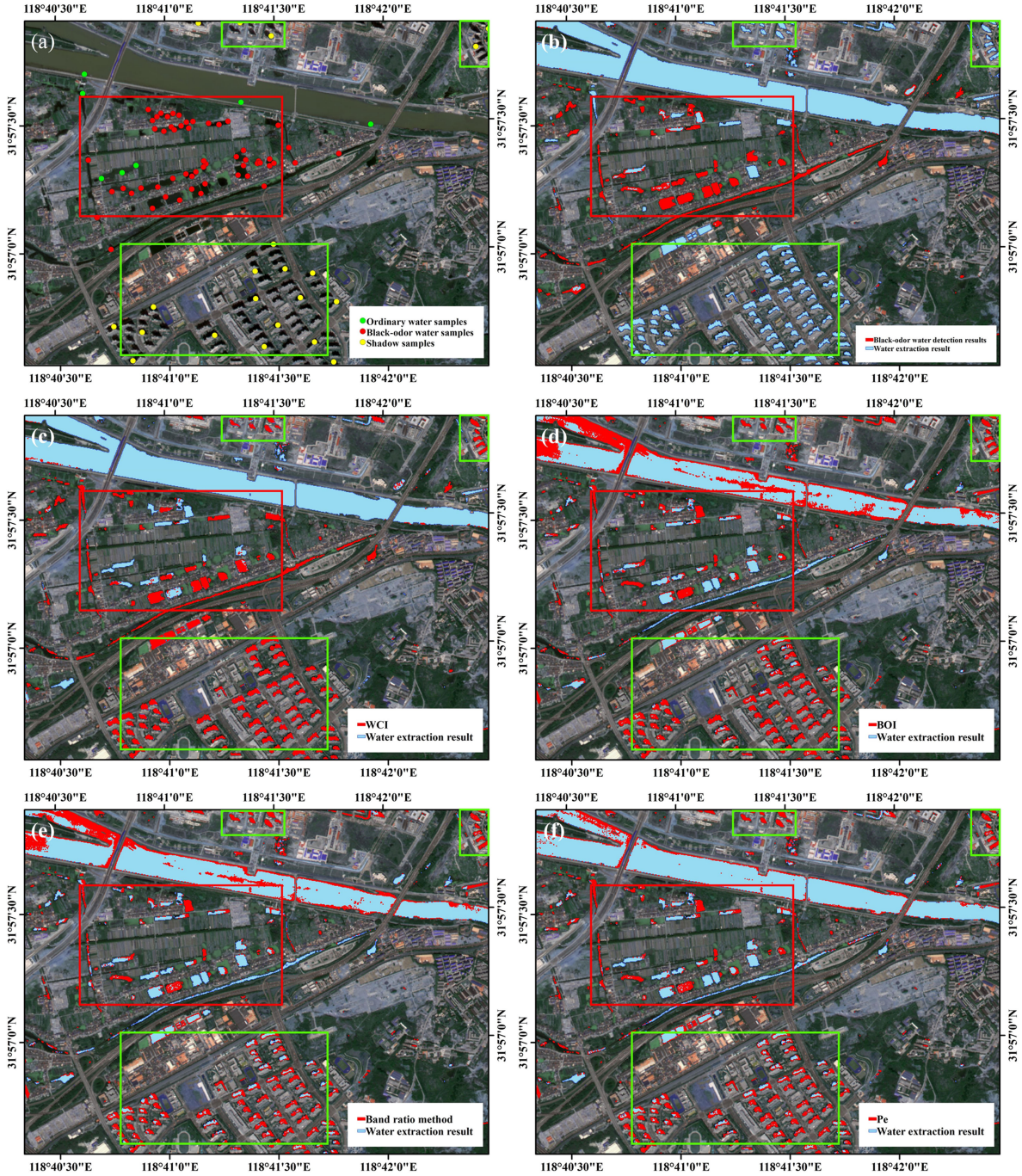

Fig. 5. Comparison of BOW detection models. (a) Distribution map of samples of BOW, ordinary water, and shadow. The green points represent the ordinary water samples, red points represent the BOW samples, and yellow points represent the shadow samples. (b) The blue area is the result of water extraction by NIR. The red area is the BOW extraction result using our model. (c–f) Results using the other models. (c) WCI, (d) BOI, (e) the band ratio method, and (f) the P_e index. The blue area and the red area represent the water extraction result and the detected BOW, respectively. Areas with dense BOW and dense shadow are shown by the red and green rectangles, respectively.

TABLE IV
COMPARISON OF THE PRECISION OF THE MODELS

Model	Function	Accuracy	False alarm rate
Proposed method	Identification method of BOW in urban multi-shadow area	85.7%	3.5%
WCI[26]	Spectral index reflects the cleanliness of water	54.8%	26.2%
BOI[25]	BOW recognition model for Shenyang, a city in northern China	60.7%	28.6%
Band ratio method[24]	BOW recognition model for Nanjing, a city in southern China	52.4%	32.1%
$\mathbf{P_e}$ method[2]	Method for water color monitoring of CIE chromaticity diagram	56%	29.8%

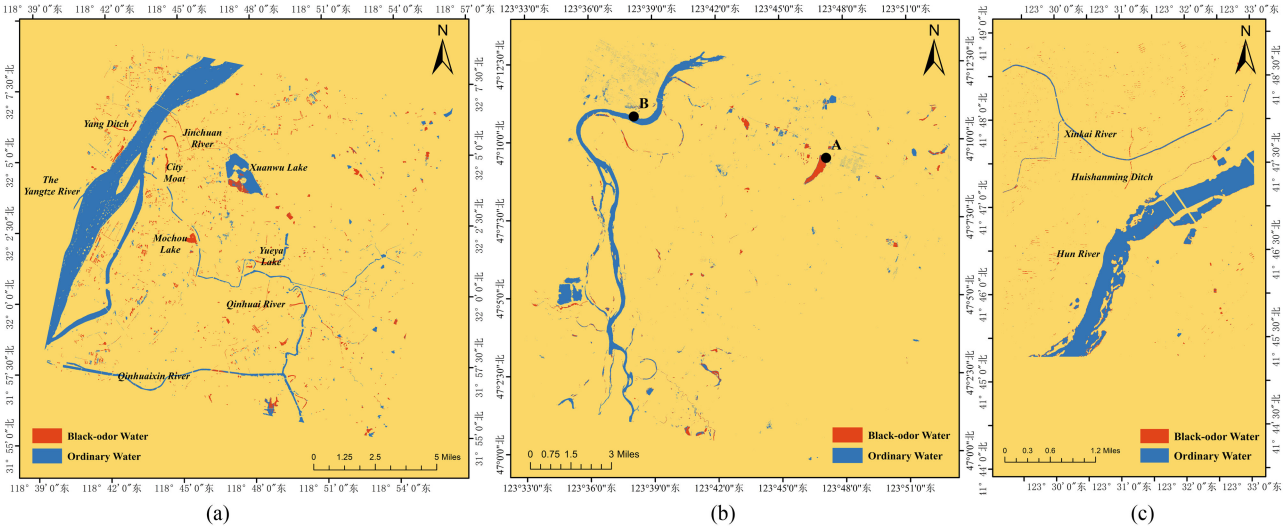

Fig. 6. (a) Remote sensing map of BOW in the main urban area of Nanjing City, Jiangsu Province. (b) Remote sensing map of BOW in the main urban area of Qiqihaer City, Heilongjiang Province. (c) Remote sensing map of BOW in the main urban area of Shenyang City, Liaoning Province.

alarm rate has a negative effect on the detection of BOW, which will increase difficulty in the centralized treatment of BOW. Compared to the other models, our model had a higher accuracy in the recognition of BOW, with a much lower error rate. In particular, none of the other models effectively distinguished BOW from building shadows, whereas our model did it very well.

D. Extended Application of the Proposed Algorithm

To verify the temporal and spatial applicability of the method in this article, remote sensing mapping of urban BOW was carried out on a large scale, and images significantly different from the above experimental seasons were selected for the experiment. The above experiment was conducted in April, which is the transition period between spring and summer. We used the GF-2 image of November 3, 2016, which serves as autumn, the transition period between summer and winter, for the experiment. In addition, our method was proposed by using a specific area, but the types of ground features in this area are very complex and basically include the common ground features in cities. Therefore, the study area can be representative of most urban areas. To verify this point, we applied the method to a larger scale BOW mapping. The GF-2 image that we chose covered most of the urban area of Nanjing. Finally, we combined the result with the field satellite synchronization sample points measured by Wen *et al*. [24] to verify the experimental results. Thus, the distribution map of BOW in the main urban area of Nanjing was obtained, as shown in Fig. 6(a). The main bodies of water in Nanjing are the Yangtze River, Xuanwu Lake, Qinhuai River, Qinhuaixin River, Jinchuan River, Mochou Lake, Yueya Lake, City Moat, and Yang Ditch. Among these, the BOW detected included Jinchuan River, Yang Ditch, City Moat, Mochou Lake, Yueya Lake, and parts of Xuanwu Lake. According to the satellite-synchronous Jinchuan River sample points measured by Wen *et al.* [24], there is a black-odor phenomenon in the Jinchuan River, which is consistent with the results of the remote sensing mapping of BOW using the method of this article. The rest of the BOW monitored is mostly stagnant water or water affected by the surrounding environment, such as river bank factory discharge and residential sewage discharge, which have a negative impact on water quality. However, because the method proposed in this article is more suitable for the extraction of urban BOW with small-scale and complex underlying conditions, partial incorrect extraction may occur in the extraction of large-scale BOW. In this case, it can be useful to consider the surrounding water environment.

The samples used for threshold analysis were all from Nanjing. To further validate the suitability of the threshold, we selected Qiqihaer and Shenyang, two typical cities in northern China, and applied the parameters that were determined in Section IV-A to remote sensing mapping of BOW. Thus, the distribution maps of BOW in the main urban area of Qiqihaer and Shenyang were obtained, as shown in Fig. 6(b) and (c). In Fig. 6(b), point B is Nenjiang River, which is a typical ordinary water [43], whereas point A in Fig. 6(b) for the typical BOW was discovered in July 2018. In fact, since 2016, a huge, severely BOW has been formed here due to the discharge of industrial wastewater. To this end, the Heilongjiang Provincial Government issued a supervision letter to the Qiqihaer Municipal Government, urging Qiqihaer to address this problem of environmental pollution [44].This is consistent with the results of the remote sensing mapping of BOW from GF-2 image of April 19, 2018. For remote sensing mapping of BOW in Shenyang, we combined the result with the field sample points measured by Yao *et al.* [25] to verify the experimental results. We selected GF-2 images covering the same area as Yao *et al.* on September 19, 2016. As shown in Fig. 6(c), Yao *et al.* collected satellite-synchronized field samples in the Huishanming ditch and Hun river. The data show that the samples from Huishanming ditch are all BOW and the samples from Hun river are all ordinary water, which is consistent with our results.

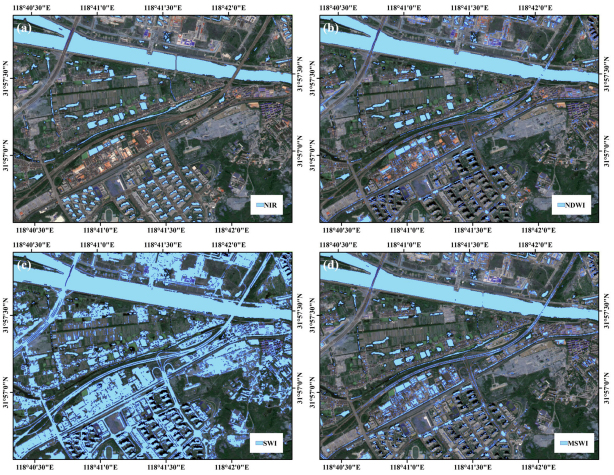

Fig. 7. Comparison of different water indices. (a) Single-band threshold method (NIR). (b) NDWI. (c) SWI. (d) MSWI. The blue area is the result of water extraction.

V. Discussion

A. Functioning of the Proposed Method for Effectively Detecting BOW From Complex Background

1) Water Extraction: Generally, BOWs are mostly narrow rivers or small ponds. Thus, it is necessary to use high-resolution remote sensing imagery for detection. In this study, we used a GF-2 satellite image. However, GF-2 imagery, with relatively little spectral information, has only the four bands of blue, green, red, and near-infrared. In addition, the complex landscape of a city, including roads, buildings, bridges, dams, shadows, and other ground objects mixed with target ground objects, increases the difficulty of detection. Hence, in this study, we first carried out a water extraction experiment. Due to the limited number of bands of the GF-2 satellite image, we tested the extraction effects of different water indices: the single-band threshold method (NIR) [41], normalized different water index (NDWI) [45], shadow water index (SWI) [46], and modified shadow water index (MSWI) [47], respectively, as shown in Fig. 7. We found that the effects of NIR and NDWI were best. As shown in Fig. 7, some roads, bridges, buildings, and shadows were incorrectly extracted by NDWI, and the land and water boundaries were badly mixed. Moreover, in the process of differentiating BOW and ordinary water, if there was a bridge across the ordinary water or a dam built on the bank, the water was likely to be categorized into BOW, resulting in a higher error rate. By contrast, with the NIR method, only shadows were mistakenly divided into water, and the influence of other ground objects on the water extraction was basically eliminated. Therefore, this study chose the method of setting the threshold value in the near-infrared band to extract water.

2) Shadow Removal: The water extraction model inhibits most of the background pixels, but there are still some dark objects that cannot be removed completely by the near-infrared band. Among these, shadow has the biggest influence on the extraction of BOW. However, BOW has the characteristics of small area and long and narrow shape, which require high image resolution. In the high-resolution remote sensing image, shadows of buildings are very similar to BOW in shape, area, and spectral information. Therefore, the removal of shadow is the most difficult problem to be solved in the extraction of BOW. To solve this problem, there are generally two ideas: the water can be extracted accurately, or the shadow can be extracted accurately. First, for accurate extraction of water, BOW presents problems such as small area, obvious water color difference, and generally low reflectance, which require high accuracy and universality of water extraction methods. The main problem affecting accuracy with the existing water extraction methods is that shadows cannot be completely distinguished from dark water, which is an even more fatal problem for BOW. In addition, the introduction of this article summarized the shortcomings of the existing methods for accurate shadow extraction, and the purpose of this work was to identify a more convenient and practical method for removing shadows.

We chose the method of water boundary constraint and calculation of the USI and zonal statistical variance to remove shadow. In the special case of BOW extraction, we can effectively manage the misclassified small shadow, reduce the false alarm rate, and also obtain a more complete boundary of BOW.

3) BOW Index: To distinguish BOW from ordinary water, we constructed an index to extract the BOW according to its spectral characteristics. We randomly selected sample points on the GF-2 image; the results after index calculation are shown in Fig. 8. The extraction index had a high degree of differentiation between BOW and ordinary water. In contrast, the other four indices did not perform as well.

B. Suitability of the BOW Index

Because of the complex causes of BOW, the water color can be roughly divided into three categories: black, brown, and green. To be specific, there are three main mechanisms for the generation of BOW, which, respectively, present three different water colors. First, exogenous organic matter and ammonia nitrogen consume oxygen in the water, so that the water is in anaerobic conditions, and the sediments in the water produce insoluble gases, which carry insoluble substances in the rising process and affect the water color. This kind of BOW color often appears black. Second, the water itself carries a large amount of sediments that affect the water color. This kind of BOW color often appears brown. Third, the stagnant water and the rising water temperature lead to the rapid propagation of algae and affect the water. This kind of BOW color often appears green. These three kinds of BOW are contained in our study area, as shown in Fig. 1(c). Our BOW index is based on the analysis of different types of BOW spectral features, so it is more universal.

In addition, our BOW index also has a clear physical meaning. The spectral characteristics of BOWs are usually related to their own substantive characteristics. The construction of the BOW detection index is based on two characteristics of its spectral curves that differ from those of ordinary water. The first characteristic is that the reflectance of ordinary water in the green band is significantly higher than that in the blue band, whereas the curve of BOW is flatter. This is due to the low

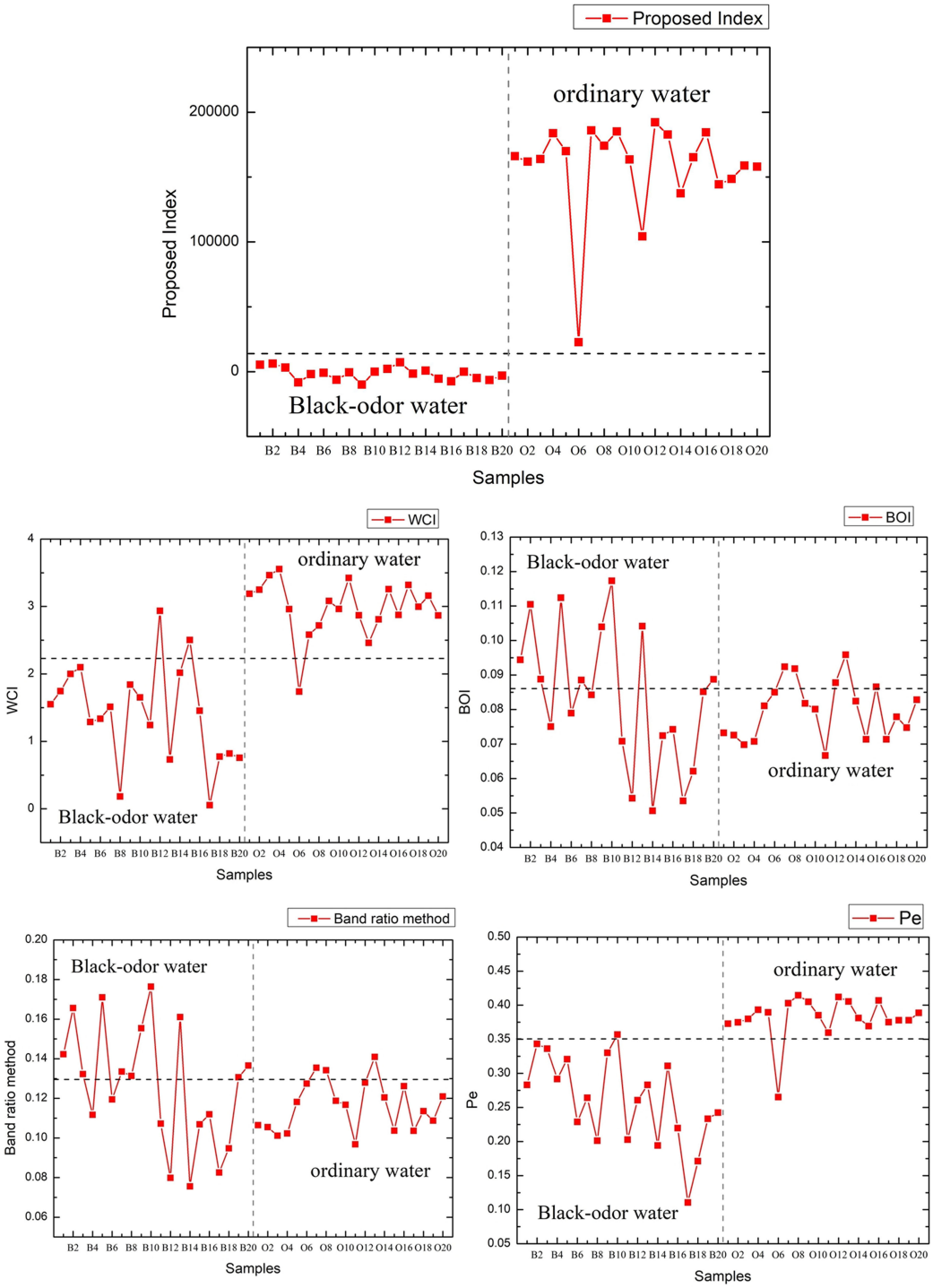

Fig. 8. Calculation results of the proposed index and the other four indices (WCI, BOI, band ratio method, and P_e, respectively) for BOW and ordinary water samples. Bi is BOW samples, and Oi is ordinary water samples. The horizontal dashed line represents the threshold.

reflectance of BOW in this visible spectrum range [48], which reduces the difference between the blue and green bands. The second characteristic is that the reflectance of ordinary water in the near-infrared band is lower than that in the green band; however, the reflectance of BOW in the near-infrared band is significantly higher, even higher than that in the green band. In fact, chlorophyll content is an important parameter for assessing water quality [49]. When algae in water are broken down in an anaerobic environment, the water becomes black and odorous. The chlorophyll remaining from the death of the algae causes high reflectance in the near-infrared band [50]. Along with the low reflectance of BOW in the green band, this characteristic can be used to distinguish BOW from ordinary water. Therefore, with the combination of the two aforementioned characteristics

of BOW, the proposed index has practical physical significance and can be used widely with good suitability for the detection of BOW.

C. Uncertainty

This study mainly aimed to identify small areas of BOW efficiently under conditions of a complex urban environment. Due to the diversity and uncertainty of spectral characteristics of BOW, undetected errors may occur. For example, because the remote sensing apparent reflectance of algae-covered BOW is characteristic of vegetation, it needs to be detected in combination with models such as the normalized difference vegetation index. The threshold value of the BOW index in this study was set using the city of Nanjing in the mid-latitude region as a reference. For other regions with climatic conditions quite different from the conditions in Nanjing, the threshold value could be adjusted appropriately according to the local conditions.

In future work, with gradual improvement of the, temporal, spatial, and spectral resolutions of satellite images, it will become possible to grade the degree of BOW through remote sensing technology. Light, moderate, and severe BOW will be able to be identified and better targeted when the government centralizes management. Furthermore, through remote sensing monitoring of the environmental conditions around the water, BOW can even be predicted. For example, by monitoring whether there is proximal point source pollution, calculating the intensity of relevant nonpoint source pollution, observing the water itself, and considering the influence of topographic factors, prediction of BOW can be realized to provide predictive data for the government and facilitate the formulation of corresponding water protection policies.

VI. Conclusion

This study detected urban BOW from a GF-2 high-resolution remote sensing image. We mainly solved three problems. The first was to realize the extraction of water from a complex environment, the second was to remove shadow effects, and the third was to develop a BOW detection method that eliminates shadow misjudgment through the analysis of hyperspectral reflectance data. Next, we used field water-quality measurements to validate our detection results and compared them with the results of four other methods. The results showed that our method can effectively suppress the influence of background information, particularly shadows, on water detection in a complex environment. The proposed BOW detection index can accurately distinguish BOW from ordinary water, and it has clear physical significance and good suitability. According to the verification results from the water quality measurements, our method reduced the error rate to 3.5% with an accuracy of 85.7%. Compared to the other four methods, our method greatly reduced the false extraction of non-BOW while still ensuring accuracy. The experiment demonstrated that our method improves the extraction of BOW in Nanjing city. It is more practical and can be used widely for the detection of urban BOW. Therefore, the method proposed in this article can provide reliable data for centralized management of urban BOW and thus improve the supervision service for urban BOW.

References

[1] Ministry Housing Urban-Rural Development, *Guideline for Urban Black and Odorous Water Treatment*, Bristol, U.K.: IOP Publishing, 2015.

[2] Q. Shen *et al.*, "A CIE color purity algorithm to detect black and odorous water in urban rivers using high-resolution multispectral remote sensing images," *IEEE Trans. Geosci. Remote Sens.,* vol. 57, no. 9, pp. 6577–6590, Sep. 2019.

[3] "Ministry of housing and urban-rural development of the people's republic of China," 2014, [Online]. Available: http://www.hcstzz.com

[4] C. I. Chang and D. C. Heinz, "Constrained subpixel target detection for remotely sensed imagery," *IEEE Trans. Geosci. Remote Sens.,* vol. 38, no. 3, pp. 1144–1159, May 2000.

[5] H. Sun, X. Sun, H. Wang, Y. Li, and X. Li, "Automatic target detection in high-resolution remote sensing images using spatial sparse coding bag-of-words model," *IEEE Geosci. Remote Sens. Lett.,* vol. 9, no. 1, pp. 109–113, Jan. 2012.

[6] D. Manolakis, C. Siracusa, and G. Shaw, "Hyperspectral subpixel target detection using the linear mixing model," *IEEE Trans. Geosci. Remote Sens.,* vol. 39, no. 7, pp. 1392–1409, Jul. 2001.

[7] J. C. Ritchie, P. V. Zimba, and J. H. Everitt, "Remote sensing techniques to assess water quality," *Photogrammetric Eng. Remote Sens.,* vol. 69, no. 6, pp. 695–704, 2003.

[8] N. M. Mattikalli and K. Richards, "Estimation of surface water quality changes in response to land use change: Application of the export coefficient model using remote sensing and geographical information system," *J. Environ. Manage.,* vol. 48, no. 3, pp. 263–282, 1996.

[9] V. E. Brando and A. G. Dekker, "Satellite hyperspectral remote sensing for estimating estuarine and coastal water quality," *IEEE Trans. Geosci. Remote Sens.,* vol. 41, no. 6, pp. 1378–1387, Jun. 2003.

[10] M. W. Matthews, S. Bernard, and K. Winter, "Remote sensing of cyanobacteria-dominant algal blooms and water quality parameters in Zeekoevlei, a small hypertrophic lake, using MERIS," *Remote Sens. Environ.,* vol. 114, no. 9, pp. 2070–2087, 2010.

[11] T. Kutser *et al.*, "Remote sensing of black lakes and using 810 nm reflectance peak for retrieving water quality parameters of optically complex waters," *Remote Sens.,* vol. 8, no. 6, pp. 497–511, 2016.

[12] M. H. Gholizadeh, A. M. Melesse, and L. N. Reddi, "A comprehensive review on water quality parameters estimation using remote sensing techniques," *Sensors,* vol. 16, no. 8, pp. 1298–1340, 2016.

[13] H. Duan, R. Ma, S. A. Loiselle, Q. Shen, H. Yin, and Y. Zhang, "Optical characterization of black water blooms in eutrophic waters," *Sci Total Environ,* vol. 482-483, pp. 174–183, Jun 2014, doi: 10.1016/j.scitotenv.2014.02.113.

[14] S. Miao *et al.*, "Characteristics of the chromophoric dissolved organic matter of urban black-odor rivers using fluorescence and UV-visible spectroscopy," *Environ. Pollut. Part B*, vol. 268, 2020, Art. no. 115763.

[15] C. Hu *et al.*, "The 2002 ocean color anomaly in the Florida bight: A cause of local coral reef decline?," *Geophysical Res. Lett.,* vol. 30, no. 3, 2003, Art. no. 140659946.

[16] C. Hu, F. E. Mullerkarger, G. A. Vargo, M. B. Neely, and E. Johns, "Linkages between coastal runoff and the Florida keys ecosystem: A study of a dark plume event," *Geophysical Res. Lett.,* vol. 31, no. 15, pp. 307–310, 2004.

[17] D. He *et al.*, "Toxicity bioassays for water from black-odor rivers in Wenzhou, China," *Environ. Sci. Pollut. Res.,* vol. 22, no. 3, pp. 1731–1741, 2015.

[18] W. H. Wang *et al.*, "Effect of calcium peroxide on the water quality and bacterium community of sediment in black-odor water," *Environ. Pollut.,* vol. 248, pp. 18–27, 2019.

[19] W. Cai *et al.*, "Vertical distribution and assemblages of microbial communities and their potential effects on sulfur metabolism in a black-odor urban river," *J. Environ. Manage.,* vol. 235, pp. 368–376, 2019.

[20] Z. P. Wang *et al.*, "Ex-situ treatment of sediment from a black-odor water body using activated sludge," *Sci. Total Environ.,* vol. 713, 2020, Art. no. 136651.

[21] J. X. Cao *et al.*, "A critical review of the appearance of black-odorous waterbodies in China and treatment methods," *J. Hazardous Mater.,* vol. 385, 2020, Art. no. 121511.

[22] Q. Shen, L. Zhu, and H. Y. Cao, "Remote sensing monitoring and screening for urban black and odorous water body: A review," *J. Appl. Ecol.*, vol. 28, no. 10, 2017, Art. no. 3433.

[23] H. X. Jin and J. Pan, "Urban black-odor water body remote sensing monitoring based on GF-2 satellite data fusion," *Sci. Technological Manage. Land Resour.*, vol. 34, no. 4, pp. 107–117, 2017.

[24] S. Wen *et al.*, "Remote sensing identification of urban black-odor water bodies based on high-resolution images: A case study in Nanjing," *Environ. Sci.*, vol. 39, no. 1, pp. 57–67, 2018.
[25] Y. Yao *et al.*, "Remote sensing identification of urban black-odor water bodies in Shenyang city based on GF-2 image," *J. Remote Sens.*, vol. 344, 2019, Art. no. 012149.
[26] J. Q. Li, J. G. Li, L. Zhu, Q. Shen, H. Y. Dai, and Y. F. Zhu, "Remote sensing identification and validation of urban black and odorous water in Taiyuan city," *J. Remote Sens.*, vol. 23, no. 4, pp. 773–784, 2019.
[27] A. M. Polidorio, F. C. Flores, N. N. Imai, A. M. G. Tommaselli, and C. Franco, "Automatic shadow segmentation in aerial color images," in *Proc. Braz. Symp. Comput. Graph. Image Process.*, 2003, pp. 270–277.
[28] H. J. Ma, Q. M. Qin, and X. Y. Shen, "Shadow segmentation and compensation in high resolution satellite images," in *Proc. Int. Geosci. Remote Sens. Symp.*, 2008, pp. 1036–1039.
[29] E. Salvador, A. Cavallaro, and T. Ebrahimi, "Cast shadow segmentation using invariant color features," *Comput. Vis. Image Understanding,* vol. 95, no. 2, pp. 238–259, 2004.
[30] H. Fang, Y. C. Wei, H. Luo, and Q. Hu, "Detection of building shadow in remote sensing imagery of urban areas with fine spatial resolution based on saturation and near-infrared information," *IEEE J. Sel. Topics Appl. Earth Observ. Remote Sens.*, vol. 12, no. 8, pp. 2695–2706, Aug. 2019.
[31] Y. Wang and S. G. Wang, "Detection and compensation of shadows in high resolution remote sensing images using PCA," *J. Appl. Sci.*, vol. 28, no. 2, pp. 136–141, 2010.
[32] J. H. Guo, Q. J. Tian, and Y. Z. Wu, "Study on multispectral detecting shadow areas and a theoretical model of removing shadows from remote sensing images," *J. Remote Sens.*, vol. 10, no. 2, pp. 151–159, 2006.
[33] Y. Mostafa and A. Abdelhafiz, "Accurate shadow detection from high-resolution satellite images," *IEEE Geosci. Remote Sens. Lett.,* vol. 14, no. 4, pp. 494–498, Apr. 2017.
[34] W. Wu, Q. Li, Y. Zhang, X. Du, and H. Wang, "Two-step urban water index (TSUWI): A new technique for high-resolution mapping of urban surface water," *Remote Sens.,* vol. 10, no. 11, 2018, Art. no. 1704.
[35] H. H. Song, B. Huang, and K. H. Zhang, "Shadow detection and reconstruction in high-resolution satellite images via morphological filtering and example-based learning," *IEEE Trans. Geosci. Remote Sens.,* vol. 52, no. 5, pp. 2545–2554, May 2014.
[36] S. H. Khan, M. Bennamoun, F. Sohel, and R. Togneri, "Automatic shadow detection and removal from a single image," *IEEE Trans. Pattern Anal. Mach. Intell.,* vol. 38, no. 3, pp. 431–446, Mar. 2016.
[37] D. S. Kim, M. Arsalan, and K. R. Park, "Convolutional neural network-based shadow detection in images using visible light camera sensor," *Sensors,* vol. 18, no. 4, pp. 960–978, 2018.
[38] P. M. Dare, "Shadow analysis in high-resolution satellite imagery of urban areas," *Photogrammetric Eng. Remote Sens.,* vol. 71, no. 2, pp. 169–177, 2005.
[39] G. Tolt, M. Shimoni, and J. Ahlberg, "A shadow detection method for remote sensing images using VHR hyperspectral and LiDAR data," in *Proc. Int. Geosci. Remote Sens. Symp.*, 2011, pp. 4423–4426.
[40] S. Luo, H. Shen, H. Li, and Y. Chen, "Shadow removal based on separated illumination correction for urban aerial remote sensing images," *Signal Process.,* vol. 165, pp. 197–208, 2019.
[41] Y. Yang and R. Z. Ruan, "Extraction of plain lake water body based on TM imagery," in *Remote Sensing Information,* vol. 3, pp. 60–64, 2010.
[42] "Cresda," 2014, [Online]. Available: http://www.cresda.com/CN/Satellite/3076.shtml
[43] "2018 Qiqihaer ecological environment status bulletin," 2018, [Online]. Available: http://www.qqhr.gov.cn/News_showGkmlNews.action?messagekey=172925
[44] "Heilongjiang: To supervise the pollution of pits and ponds in Ang'angxi district of Qiqihar city," 2018, [Online]. Available: http://k.sina.com.cn/article_5044281310_12ca99fde02000i5gp.html
[45] S. K. Mcfeeters, "The use of the normalized difference water index (NDWI) in the delineation of open water features," *Int. J. Remote Sens.,* vol. 17, no. 7, pp. 1425–1432, 1996.
[46] J. Bai, X. Chen, J. Li, L. Yang, and H. Fang, "Changes in the area of inland lakes in arid regions of central Asia during the past 30 years," *Environ. Monit. Assessment,* vol. 178, no. 1, pp. 247–256, 2011.
[47] W. Q. Chen, J. L. Ding, L. I. Yanhua, and Z. Y. Niu, "Extraction of water information based on China-made GF-1 remote sense image," *Resour. Sci.,* vol. 9, no. 4, 2015, Art. no. 189.
[48] C. J. Lv, H. J. Gao, X. J. Li, Y. H. Song, and Q. Shen, "DOM components and optical properties of black-odorous rivers in Shenyang city," *Chin. J. Environ. Eng.*, vol. 13, no. 3, pp. 61–70, 2019.
[49] A. Sabattomala *et al.*, "Application of Hyspex hyperspectral images for verification of a two-dimensional hydrodynamic model," *Eur. J. Remote Sens.,* vol. 51, no. 1, pp. 637–649, 2018.
[50] X. W. Li, Z. C. Niu, S. Jiang, and Y. Jin, "Satellite remote sensing monitoring of black color water blooms in lake Taihu," *Admin. Technique Environ. Monit.*, vol. 28, no. 27, pp. 12–17, 2012.

Taixia Wu received the M.S. degree in cartography and GIS from the College of Urban and Environmental Sciences, Northeast Normal University, Changchun, China, in 2006, and the Ph.D. degree in remote sensing from Peking University, Beijing, China, in 2010.

He is currently a Professor with the School of Earth Sciences and Engineering, Hohai University, Nanjing, China. His research interests include hyperspectral remote sensing and water remote sensing applications.

Mengyao Li is currently working toward the M.S. degree in cartography and geographical information engineering with the School of Earth Sciences and Engineering, Hohai University, Nanjing, China.

Her research interests include remote sensing of water resources environment and nonpoint source pollution.

Shudong Wang received the Ph.D. degree in cartography and GIS from the State Key Laboratory of Remote Sensing, Institute of Remote Sensing and Digital Earth, Normal University, Beijing, China, in 2007.

He is currently an Associate Research Fellow with the Aerospace Information Research Institute, Chinese Academy of Sciences, Beijing, China. His research interests include optical remote sensing and its application in ecological and environment field.

Yingying Yang is currently working toward the Ph.D. degree in ecological remote sensing with the School of Earth Sciences and Engineering, Hohai University, Nanjing, China.

Her research interests include remote sensing of environment and forest monitoring.

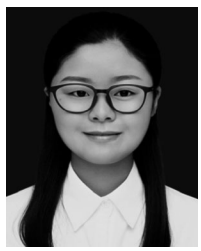

Shan Sang is currently working toward the M.S. degree with the School of Earth Sciences and Engineering, Hohai University, Nanjing, China.

Her research interests include remote sensing assessment of ecological environment and quantitative remote sensing.

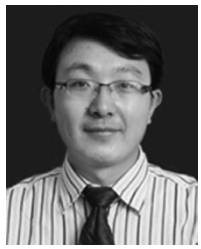

Dongzhen Jia received the B.Eng. degree in surveying and mapping engineering, and the M.S. and the Ph.D. degrees in geodesy from Hohai University, Nanjing, China, in 2003, 2006, and 2018, respectively.

From December 2007 to December 2008, he was a Visiting Researcher with Nanyang Technological University, Singapore. He is currently a Lecturer with the School of Earth Science and Engineering, Hohai University. His research interests include deformation monitoring and 3-D laser scanning applications.